Separation Science and Technology
Publication details, including instructions for authors and subscription information:
http://www.informaworld.com/smpp/title~content=t713708471

Study of a Nanoparticle Charger Containing Multiple Discharging Wires in a Tube

C. J. Tsai[a]; S. C. Chen[a]; H. L. Chen[a]; H. M. Chein[b]; C. H. Wu[a]; T. M. Chen[b]
[a] Institute of Environmental Engineering, National Chiao Tung University, Hsin Chu, Taiwan [b] Energy and Environment Research Laboratories, Industrial Technology Research Institute, Hsin Chu, Taiwan

To cite this Article Tsai, C. J. , Chen, S. C. , Chen, H. L. , Chein, H. M. , Wu, C. H. and Chen, T. M.(2008) 'Study of a Nanoparticle Charger Containing Multiple Discharging Wires in a Tube', Separation Science and Technology, 43: 13, 3476 — 3493
To link to this Article: DOI: 10.1080/01496390802219034
URL: http://dx.doi.org/10.1080/01496390802219034

Separation Science and Technology, 43: 3476–3493, 2008

ISSN: 0149-6395 print/1520-5754 online
DOI: 10.1080/01496390802219034

Taylor & Francis
Taylor & Francis Group

Study of a Nanoparticle Charger Containing Multiple Discharging Wires in a Tube

C. J. Tsai,[1] S. C. Chen,[1] H. L. Chen,[1] H. M. Chein,[2] C. H. Wu,[1] and T. M. Chen[2]

[1]Institute of Environmental Engineering, National Chiao Tung University, Hsin Chu, Taiwan

[2]Energy and Environment Research Laboratories, Industrial Technology Research Institute, Hsin Chu, Taiwan

Abstract: A unipolar charger containing multiple discharging wires in a tube (inner diameter: 50 mm) was developed and tested in order to increase the aerosol flow rate and the charging efficiency of nanoparticles. Four gold wires of 25 μm in diameter and 15 mm in length were used as the discharging electrodes to generate positive ions (N_i) from 2.72×10^8 ions/cc to 3.87×10^9 ions/cc in concentration at the discharging voltage of $+4.0 \sim +10$ KV. Monodisperse NaCl particles of 10∼50 nm in diameter were used to test the charging efficiency and the particle loss of charged particles with different aerosol flow rates, corona voltages and sheath flow rates. The sheath air near the tube wall was found to increase the extrinsic charging efficiency, and the highest efficiency was obtained at +6.0 KV discharging voltage, 10 L/min aerosol flow rate and 9 L/min sheath flow rate. The extrinsic charging efficiency increased from 10.6% to 74.2% when the particle diameter was increased from 10 to 50 nm. The TDMA (tandem differential mobility analyzer) method was used to determine the charge distribution and the mean charge per particle and it was found that the Fuchs charging theory corrected for the extrinsic charging efficiency matched with the experimental data very well.

Keywords: Charging efficiency, nanoparticles, unipolar charger

Received 10 October 2007; accepted 6 April 2008.

Address correspondence to C. J. Tsai, Institute of Environmental Engineering, National Chiao Tung University, Hsin Chu, Taiwan. Tel.: +886-3-5731880; Fax: +886-3-5727835. E-mail: cjtsai@mail.nctu.edu.tw

INTRODUCTION

Particle charging is very important to particle measurement, such as particle sizing by the differentially mobility analyzer (1) and to particle control, such as the removal of particles by the electrostatic precipitator (2). However, for nanosized particles, charging efficiency is low. As a result, many researchers have devoted their efforts to develop efficient aerosol chargers for nanoparticles.

Aerosol particles can be charged by either bipolar or unipolar charging. In the case of bipolar charging, two competing processes, namely charging and neutralizing, lead to low charging efficiency which is only 4% for 10 nm particles when they are positively charged, or 6% when they are negatively charged (3). The unipolar charging technique is aimed at achieving higher nanoparticle charging efficiency. Wiedensohler et al. (4) used an alternative electric field in the charging region to reduce particle loss to the walls. The bipolar ions were generated by a radioactive source, Cm^{244}, placed in two opposite boxes. An alternative electric field was applied between screen openings near each box to draw unipolar ions into the charging zones at the center. The charged particles moved in a zigzag manner under the influence of the alternative electric field. The extrinsic changing efficiency was 4% for 10 nm particles.

To increase the charging efficiency, Chen and Pui (5) designed a unipolar charger with parallel aerosol and ion flow configuration to avoid particle loss. Desirable unipolar ions were separated by a weak electric field from bipolar ions generated by four Po^{210} radioactive sources. The design further used sheath air surrounding the aerosol flow to reduce particle loss. As a result, the extrinsic charging efficiency was greatly enhanced and up to 22% for 3 nm, 48% for 5 nm, and 65% for 10 nm positively charged particles was reported. So far, this design has the highest extrinsic charging efficiency among all unipolar charger designs. Later on, Kruis and Fissan (6) developed a Twin Hawitt type which used two Au wires placed in different boxes to generate unipolar ions. An alternative field was applied to draw unipolar ions from boxes into the charging zone. No sheath air was added. The extrinsic charging efficiency achieved was about 30% for 10 nm positive particles. Later on, another diffusion charger was constructed and evaluated by Biskos et al. (7). The charger has two concentric electrodes with a corona wire placed along the axis. The ions move from the central toward the inner perforated electrode due to high electric field. Afterward, an AC voltage was applied on the outer electrode to increase ion penetration and reduce particle loss on the walls. The extrinsic charging efficiency achieved was 25% and 60% for 10 nm and 20 nm positively charged particles, respectively.

Laschober et al. (8) tested a corona based unipolar charging unit and found the yield of singly charged particles to be two to four times higher compared to bipolar charging. Alonso et al. (9) proposed a corona charger with a simple configuration. The corona discharge takes place around a sharp-point stainless steel electrode, and aerosols collide directly with unipolar ions. The extrinsic charging efficiency of nanoparticles is similar to that of other complex designs.

The purpose of this work is to design another simple charger: a wire-in-tube unipolar charger with multiple discharging wires, and evaluate the extrinsic charging efficiency at different operating conditions aiming at increasing the aerosol flow rate and charging efficiency. Similar attempt to increase the aerosol flow of the charger was published by Cheng et al. (10) but the extrinsic charging efficiency was not reported. In this study, the charge distribution and mean charge of nanoparticles were also measured and compared with that predicted using Fuchs charging theory (11).

PRESENT UNIPOLAR CHARGER DESIGN

Figure 1 shows the schematic diagram of the newly developed unipolar charger. The charger has an inner Teflon core to hold four 25 μm gold wires to which high voltage is applied. The outer stainless steel casing is grounded. The initial length of the wires, 26 mm, was found to be too long to result in too much particle loss. Therefore a short Teflon tube underneath the Teflon core was added to cover part of the wires so that the effective length of the wires is reduced to 15 mm. The space beneath the inner Teflon disc was filled by an aluminum cylinder to minimize the dead space and possible diffusion loss of particles. Gold wires were used since they lasted for more than six months (12). Only high positive voltage was used in this study. The positive corona was generated within the annulus between the gold wires and the stainless steel casing where aerosol charging took place simultaneously. In order to reduce charged particle loss in the charging zone, a clean sheath air was introduced from the 0.5 mm slit formed by the aluminum shroud and the outer casing.

The corona current I versus corona voltage V was measured using the setup shown in Fig. 2. An inner stainless steel ring installed near the stainless steel casing was connected to a Keithley Model 6485 picoammeter (Keithley Instrument, Inc., Ohio, USA) to measure the corona current. In the present work, the corona starting voltage, V_c, was assumed to have the following form:

$$V_c = \gamma E_b r_1 \ln\left(r_2/r_1\right) \tag{1}$$

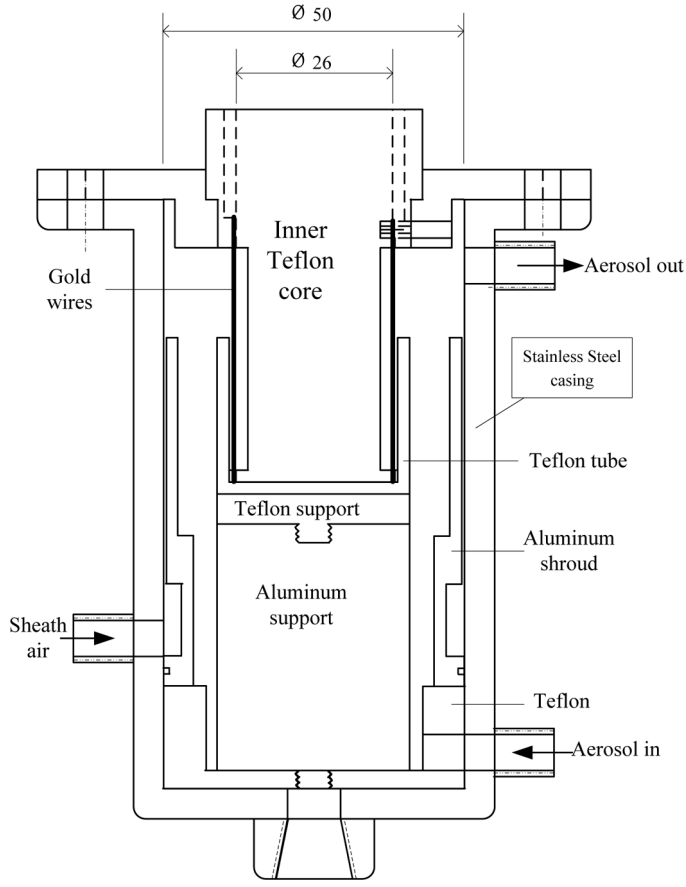

Figure 1. Schematic diagram of the present unipolar charger (unit: mm).

where $E_b = 3000 + 127d_1^{-1/2}$ is the breakdown voltage (KV/m) (13), d_1 and r_1 are the diameter and radius of the discharging wires; r_2 is the distance between the outer casing and discharging wires (11.25 mm). γ is a fitting parameter which was found to be 1.5 to fit the data best in this study. The fitting parameter γ is needed since the current design is different from the single wire-in-tube configuration. The ion concentration N_i was assumed to be related to the corona current I as:

$$N_i = \frac{I \ln\left(r_2/r_1\right)}{\chi 2\pi V Z_i Le} \tag{2}$$

where χ is a fitting parameter which was later found to be 2.5 for the best fitting with the data. The corona voltage V is

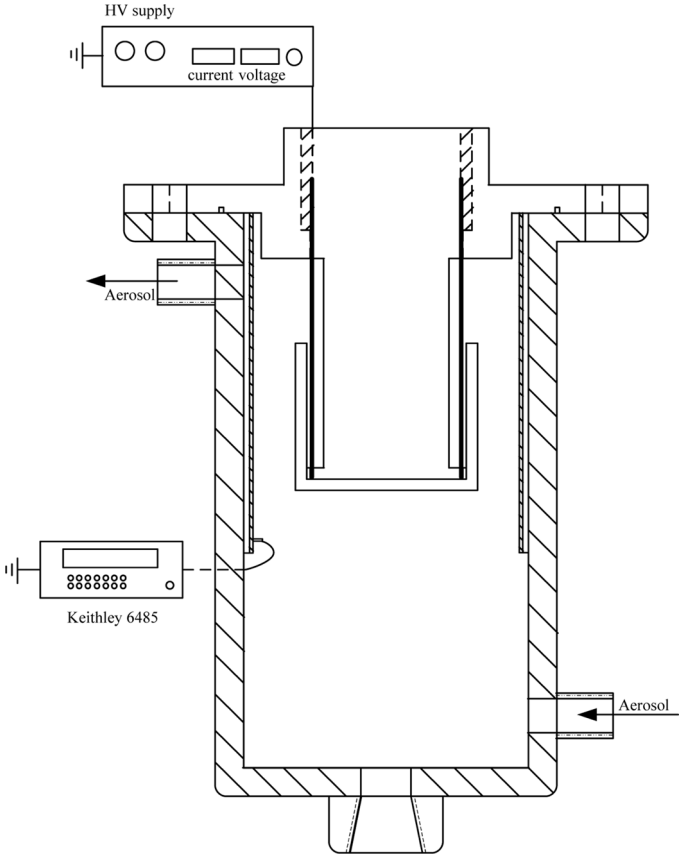

Figure 2. Schematic diagram of measuring the corona current.

$$V = V_c + E_b\, r_1 \left[\sqrt{1+\theta} - 1 - \ln\left(\frac{1+\sqrt{1+\theta}}{2} \right) \right] \tag{3}$$

and

$$\theta = \frac{I\, r_2^2}{\chi 2\pi\, \varepsilon_0\, Z_i\, E_b^2\, r_1^2} \tag{4}$$

In the above equations, Z_i is the electrical mobility of positive ions ($1.4 \times 10^{-4}\,\mathrm{m^2/V\text{-}sec}$), L is the length of the discharging wires; e is the elementary charge (1.6×10^{-19} C), ε_0 is the permittivity of a vacuum ($8.85 \times 10^{-12}\,\mathrm{C^2/N\text{-}m^2}$).

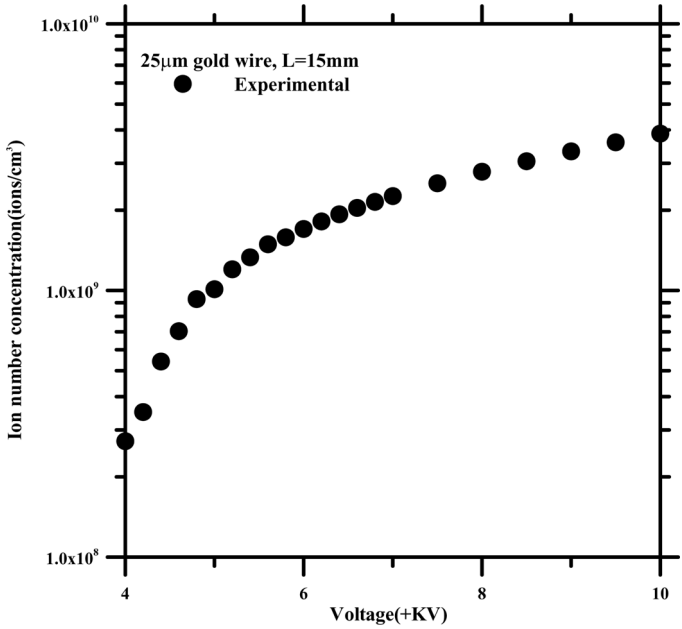

Figure 3. Ion number concentration variation with the corona voltage.

The ion number concentration variation with the applied positive voltage is shown in Fig. 3. When the positive corona voltage increases from +4.0 KV to +10 KV, ion concentration will increase from 2.72×10^8 to 3.87×10^9 ions/cm^3, as calculated by Eq. (2). The residence time of the aerosol flow in the charging zone is 0.68 to 0.14 sec when the aerosol flow rate is 2 L/min to 10 L/min. These ion concentration values are higher than the concentrations in previous researches. For example, N_i in Chen and Pui (5) is 2.56×10^7 ions/cm^3 and the maximum N_i in Kruis and Fissan (6) is about 8×10^7 ions/cm^3. As a result, diffusion charging by unipolar ions will be more efficient under the same conditions as long as the electrostatic loss of particles is kept small.

EXPERIMENTAL

Charging Performance Evaluation

Figure 4 shows the schematic diagram of the experimental setup used for measuring charging efficiency and the particle loss of the charger in the laboratory. Nano-sized NaCl particles generated by the evaporation-condensation technique were neutralized by an electrostatic neutralizer

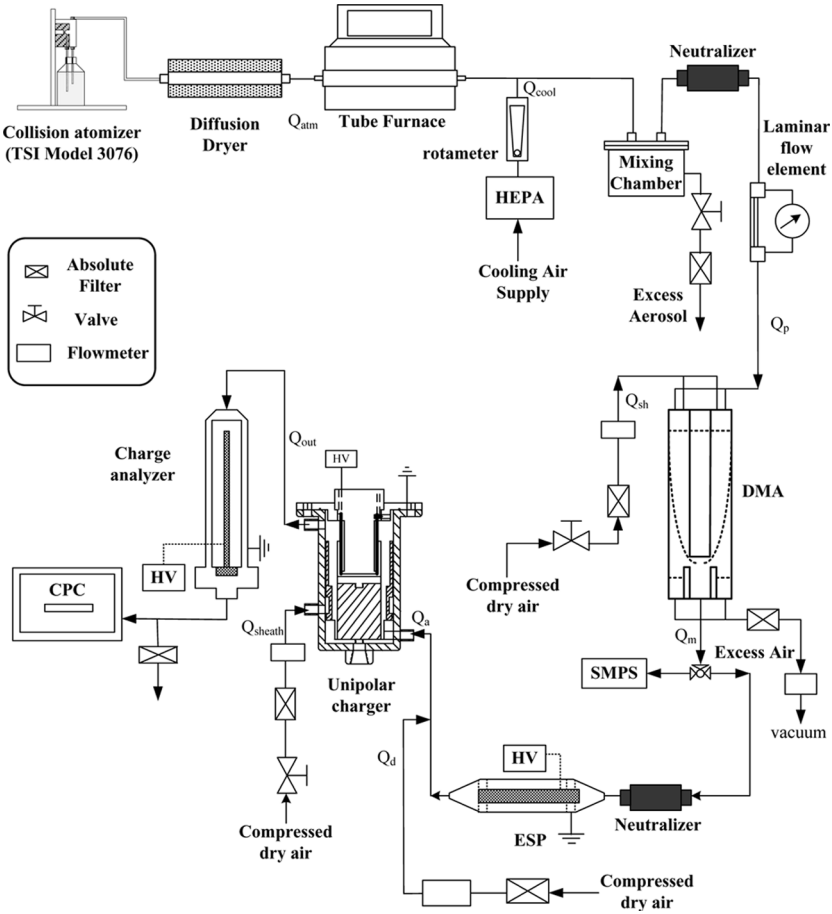

Figure 4. Schematic diagram of the experimental setup.

(model 3077, TSI Inc.), and classified in the Nano-DMA (Nano-differential mobility analyzer, model 3085, TSI Inc.). The singly charged monodisperse particles were then passed through another TSI 3077 neutralizer and an electrostatic precipitator to remove all charged particles. Only uncharged particles were introduced into the unipolar charger. Before entering the charger, an additional clean air was mixed with uncharged particles to increase the aerosol flow rate. In the charging zone, sheath air could be introduced from the 0.5 mm wide annular slit along the inner wall of the charger. After charged aerosol flow exited the charger, it was further introduced into a charge analyzer designed based on Tsai et al.

(14) and Forsyth et al. (15) and a CPC (condensation particle counter, model 3022, TSI Inc.) to measure particle electrostatic charges.

There are four parameters used for evaluating the charging performance of a unipolar charger, including intrinsic charging efficiency (η_{int}), extrinsic charging efficiency (η_{ext}), electrostatic loss (L_{el}), and diffusion loss (L_d^0), which are calculated by the following expressions (16):

$$\eta_{\text{int}} = f\frac{C_{out,OFF} - C_{out}^0}{C_{in}} \tag{5}$$

$$\eta_{ext} = f\frac{C_{out,ON} - C_{out}^0}{C_{in}} \tag{6}$$

$$L_{el} = f\frac{C_{out,OFF}C_{in}C_{out,ON}}{C_{in}} \tag{7}$$

$$L_d^0 = 1 - f\frac{C_{out,OFF}}{C_{in}} \tag{8}$$

where the dilution factor f is equal to the ratio of the outlet to the inlet aerosol flow rates of the charger, C_{in} is the particle number concentration before the charger, $C_{out,OFF}$ is the particle number concentration when no voltage is applied on the charger and charge analyzer, $C_{out,ON}$ is the particle number concentration after the charger while no voltage is applied on the charge analyzer, C_{out}^0 is the particle number concentration after the charger when a sufficiently high voltage is applied on the charge analyzer to remove all charged particles.

Charge Distribution and Average Charge Measurement

Similar to Alguacil and Alonso (17), a Tandem DMA system was used for measuring the charge distribution and the average charge of charged particles. The schematic diagram is shown in Fig. 5. When monodisperse particles were charged in the unipolar charger, a DMA coupled with a CPC were used to scan the size distribution of the charged particles at the exit of the charger. The resulting distributions contain multiple

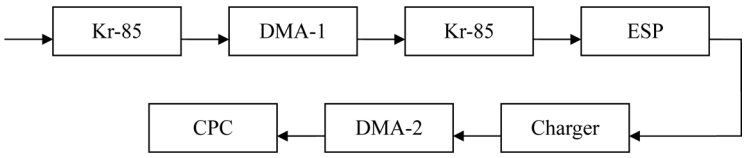

Figure 5. Experimental setup for measuring the particle charge distribution and average charge.

modes with the peaks appearing at mobility values which are integral multiples of the mobility of singly charged particles. Under each discharging voltage, there is a corresponding charge distribution of charged particles. Each peak on the curve represents a specific number of elementary charges per particle. The relative fractions of multiply charged particles are determined from the relative areas under their corresponding peaks, termed as ''extrinsic charge distributions''. Finally, the average charge per particles is calculated by the product of the extrinsic charge distribution and the corresponding number of elementary charges per particle. The average charge values are then compared with the theoretical predictions based on Fuchs limiting-sphere charging theory

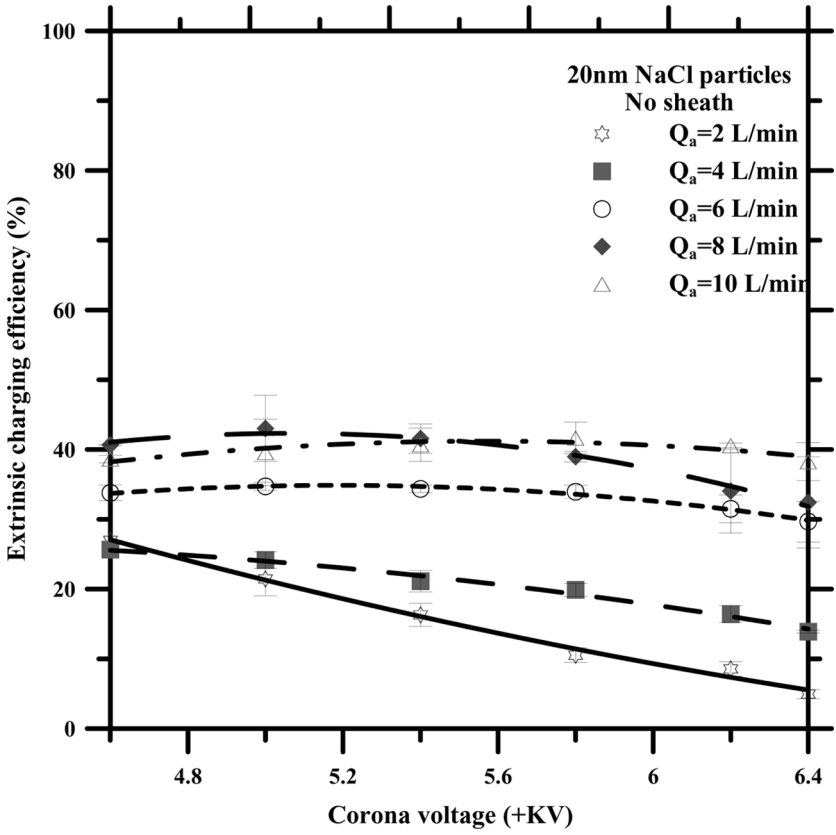

Figure 6. Extrinsic charging efficiency as a function of aerosol flow and corona voltage. The discharging voltage and aerosol flow rate are +5.4 KV and 4 L/min, respectively.

in the transition regime (11). In the charger, the concentration of uncharged particles (n_0) and charged particles with p charges (n_p) can be obtained from the following governing equation:

$$\frac{dn_0}{dt} = -\beta_0^+ n_0 N^+ \tag{9}$$

$$\frac{dn_p}{dt} = \beta_{p-1}^+ n_{p-1} N^+ - \beta_p^+ n_p N^+ \tag{10}$$

where N^+ is the ion concentration and t is time. β_0^+ and β_p^+ are the combination coefficients between particles ions and particles with zero or p charges, respectively, calculated using the Fuchs charging theory (11).

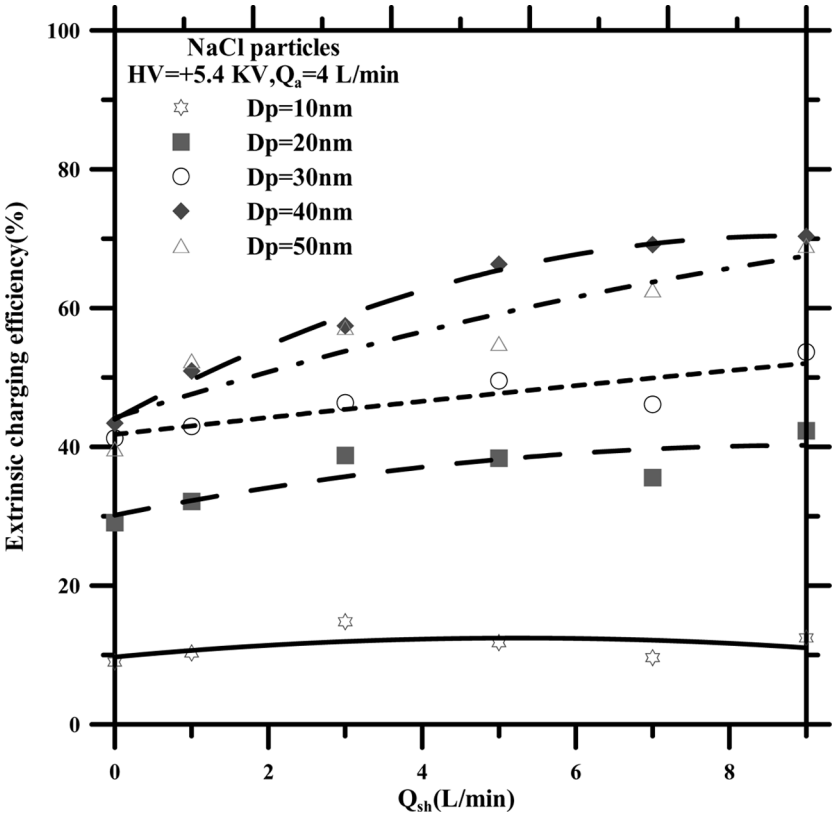

Figure 7. Extrinsic charging efficiency as a function of sheath flow rate. The discharging voltage and aerosol flow rate are +5.4 KV and 4 L/min, respectively.

RESULTS AND DISCUSSION

Charging Efficiency and Particle Loss

Effect of Aerosol Flow Rate, no Sheath Air Flow

The particle charging efficiency will vary with the aerosol flow rate and the corona voltage. Figure 6 shows the extrinsic charging efficiency for 20 nm NaCl particles as an example. For aerosol flow below 4 L/min, the extrinsic charging efficiency decreases from 26% with increasing corona voltage from 4.6 to 6.4 KV. At higher aerosol flow than 4 L/min, the corona voltage does not affect the extrinsic charging efficiency very much and the efficiency maintains between 30 to 40%. The highest extrinsic charging efficiency is obtained at the highest aerosol flow rate of 10 L/min corresponding to the shortest aerosol residence time of

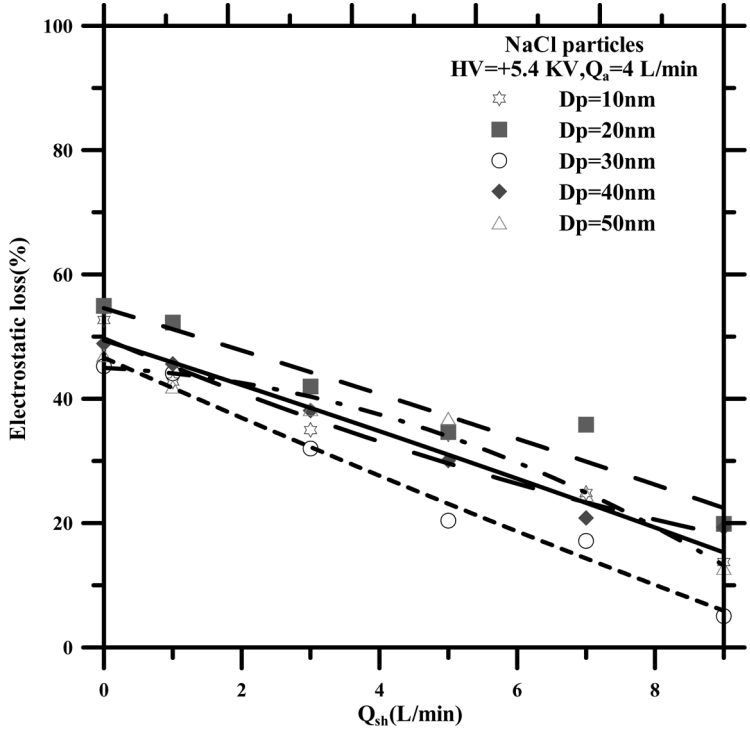

Figure 8. Electrostatic loss as a function of sheath flow rate. The discharging voltage and aerosol flow rate are +5.4 KV and 4 L/min, respectively.

0.14 sec. Experimental data of particle electrostatic loss show that as the corona voltage increases, the loss also increases which offsets the increase of the intrinsic charging efficiency. As a result, the corona voltage does not affect the extrinsic charging efficiency very much when the aerosol flow rate is greater than 4 L/min.

Effect of Sheath Air Flow Rate

To reduce the electrostatic loss, sheath air was added. The results of extrinsic charging efficiency are shown in Fig. 7 for 10–50 nm NaCl particles at 4 L/min aerosol flow rate, +5.4 V corona voltage, and different sheath flow rates from 0 to 9L/min. Depending on the particle diameter, the extrinsic charging efficiency of particles larger than 20 nm ranges from 30 to 70%, which is enhanced by about 10–30% by using the sheath air flow. This increase is due to the prevention of charged

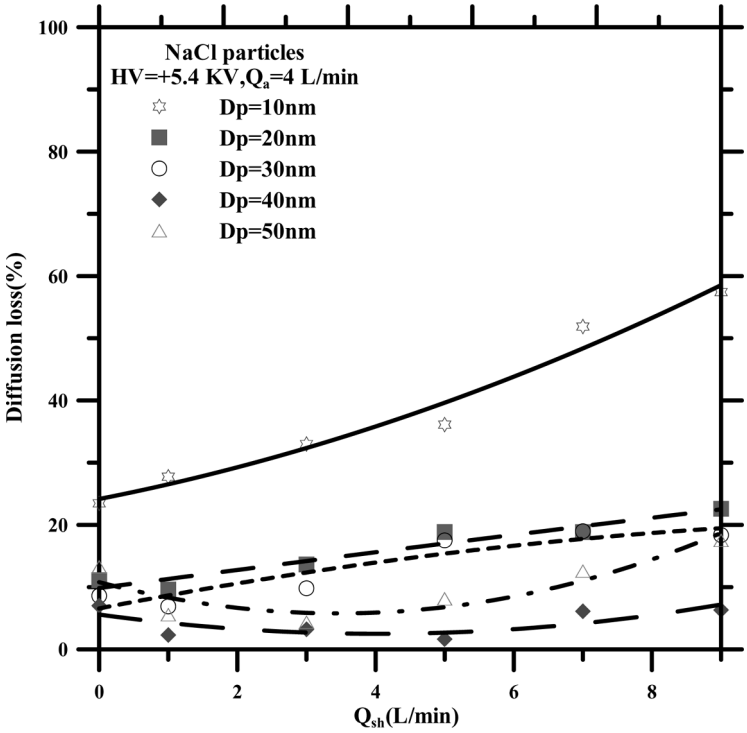

Figure 9. Diffusion loss as a function of sheath flow rate. The discharging voltage and aerosol flow rate are +5.4 KV and 4 L/min, respectively.

particle deposition on the wall and the reduction of electrostatic loss, as shown in Fig. 8. Without using the sheath air, the loss is severe which ranges from 45 to 50% for particles from 10 to 50 nm. The loss decreases almost linearly to 5 to 20% as the sheath flow is increased to 9L/min.

For 10 nm particles, the extrinsic efficiency does not seem to be affected by the sheath flow rate as shown in Fig. 7. The reason is due to the increasing diffusion loss of 10 nm particles with increasing sheath air flow rate as shown in Fig. 9. However, for other particle sizes, the diffusion loss remains below 20% and does not change very much with the sheath air flow rate. Such differences are suspected to be due to the lack of strength or non-uniformity of the sheath air flow velocity as it exists from the 0.5 mm slit. This sheath air problem will be investigated further to better explain the data shown in Fig. 9 and reduce the particle loss in the charger.

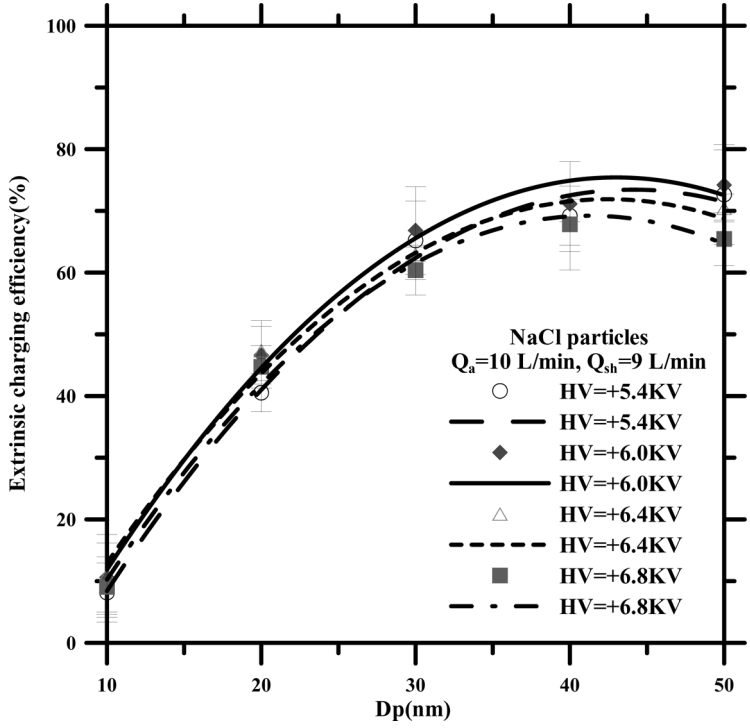

Figure 10. Extrinsic charging efficiency as a function of particle diameter. The aerosol flow rate and sheath flow rate are 10 L/min and 9 L/min, respectively.

According to the previous results, higher extrinsic charging efficiency can be obtained with a sufficiently high discharging voltage at high aerosol flow and sheath air flow rates. Experiment was therefore conducted at 10 L/min aerosol flow and 9 L/min sheath flow at four different discharging voltages from 5.4 to 6.8 KV and results are shown in. Fig. 10. The best extrinsic charging efficiency of 10.6 to 74.2% for particles ranging from 10–50 nm is seen to occur at + 6.0 KV. The charging efficiency at other corona voltages is similar but slightly lower. Comparing with the maximum extrinsic charging efficiency attainable in previous designs, the present charger is about 20–30% lower. The differences are due to large particle loss that still exists in the present charger. There is 15% electrostatic loss and 10% diffusion loss for particles above 20 nm, and severe diffusion loss of 50% for 10 nm particles. Therefore, the loss needs to be further reduced. One possible solution is to increase the sheath air

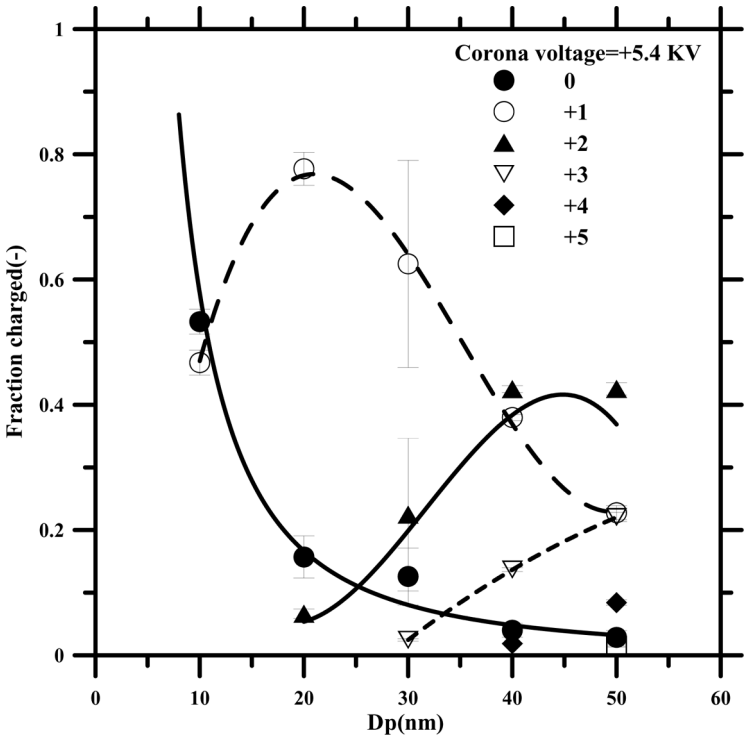

Figure 11. Charge distribution as a function of particle diameter. The discharging voltage is +5.4 KV.

velocity and uniformity by reducing the gap between the aluminum shroud and the tube wall.

Charge Distribution and Mean Number of Charges per Particle

The charge distributions as a function of particle size at + 5.4 KV discharging voltage are shown in Fig. 11. It can be seen that nearly all 10 nm particles are singly charged. For larger particles, the fraction of multiply charged particles becomes higher. Some fraction of particles carrying five charges is measured for 50 nm particles. For other operating conditions, there will be corresponding charge

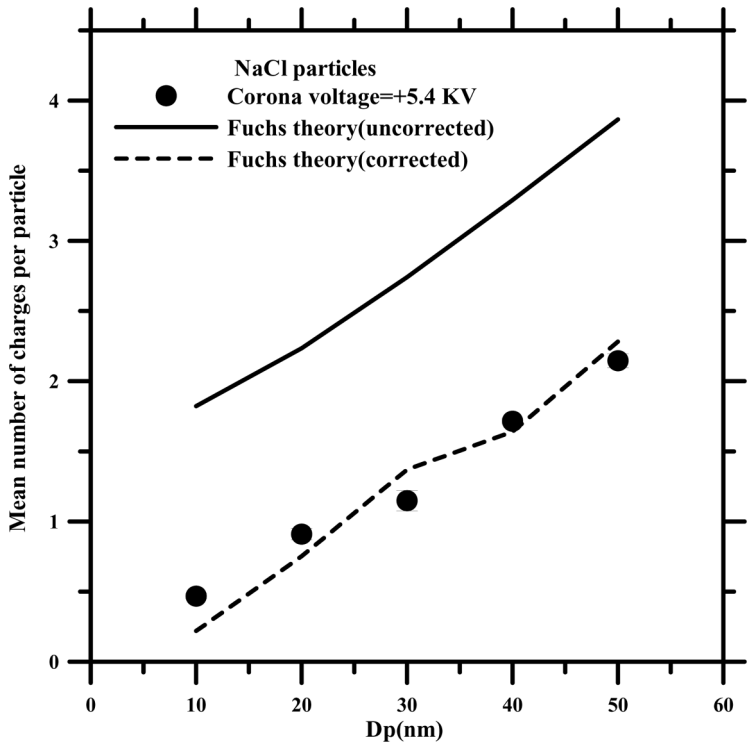

Figure 12. Mean number of elementary charges per particles as a function of particles diameter. Comparison between experimental data and theoretical results calculated using Fuchs charging theory (uncorrected—without considering extrinsic charging efficiency; corrected—considering extrinsic charging efficiency).

distributions. The mean average charge per particle is calculated by summing the product of the number fraction of a certain multiple charged particle with the corresponding number of elementary charges and the results are shown in Fig. 12. It shows the mean average charge of particles increases from 0.46 to 2.2 with increasing particle diameter from 10 to 50 nm. The comparison with the values obtained using Fuchs charging theory but uncorrected for the extrinsic charging efficiency indicates the agreement is not good. Since the experimental results were acquired at the exit of the charger, the average charge predicted by using Fuchs theory was corrected by multiplying it with the extrinsic charging efficiency. After correction, the experimental data show a very good agreement with Fuchs theory.

CONCLUSION

A unipolar charger with multiple discharging wires was developed and tested for the purpose of increasing the aerosol flow rate and enhancing the charging efficiency of nanoparticles. The charging performance measurement was carried out under different operation conditions of different aerosol flow rates, corona voltages, and sheath flow rates. The operating voltage of the charger ranged from $+4.0 \sim +10$ KV which corresponded to 2.72×10^8 ions/cc to 3.87×10^9 ions/cc positive ion concentration. When there was no sheath air flow, increasing the corona voltage resulted in a higher ion number concentration. However, the higher electrostatic loss occurred due to a stronger electrical field strength. By shortening the residence time in the charging region by increasing the aerosol flow from $2 \sim 10$ L/min (residence time from 0.68 to 0.14 sec), the extrinsic charging efficiency was found to increase with the maximum efficiency obtained at 10 L/min. The sheath air flow near the tube wall increased the extrinsic charging efficiency by reducing the particle electrostatic loss. The optimal operation condition for particles from $10 \sim 50$ nm in diameter with the highest extrinsic charging efficiency from $14\% \sim 77\%$ was obtained at $+6.0$ KV discharging voltage, 10 L/min aerosol flow, and 9 L/min sheath flow. The extrinsic charging efficiency can be improved further by reducing the gap of the slit and increasing the sheath air velocity and uniformity. The TDMA method was further used to analyze the charge distribution and the mean average charge of particles. The experimental data show good agreement with the theoretical results based on Fuchs charging theory taking into account the extrinsic charging efficiency.

In the future, it is worthwhile to improve the extrinsic charging efficiency further by increasing the sheath air velocity. Also it is useful to investigate the possibility of using this unipolar charging device as a substitute for the widely used diffusion charging device which uses a radioactive source.

ACKNOWLEDGEMENTS

The authors would like to express thanks to the Taiwan NSC (Project no. NSC-93-2211-E-009-015) and the Industrial Technology Research Institute (contract no. 3000141829) for the financial support of this project.

REFERENCES

1. Kuntson, E.O.; Witby, K.T. (1975) Aerosol classification by electric mobility: Apparatus, theory, and applications. *J. Aerosol Sci.*, *6*: 443–453.
2. Huang, S.H.; Chen, C.C. (2002) Ultrafine aerosol penetration through electrostatic precipitator. *Environ. Sci. Technol.*, *36*: 4625–4632.
3. Reischl, G.P.; Mäkelä, J.M.; Necid, J. (1996) Bipolar charging of ultrafine particles in the size range below 10 nm. *J. Aerosol Sci.*, *27*: 931–949.
4. Wiedensohler, A.; Buscher, P.; Hasson, H.C.; Martinsson, B.G.; Stratmann, F.; Ferron, G.; Busch, B. (1994) A novel unipolar charger for ultrafine aerosol particles with minimal particle losses. *J. Aerosol Sci.*, *25*: 639–649.
5. Chen, D.R.; Pui, D.Y.H. (1999) A high efficiency, high throughput unipolar aerosol charger for nanoparticles. *J. Nanoparticle Res.*, *1*: 115–126.
6. Kruis, F.E.; Fissan, H. (2001) Nanoparticle charging in a twin Hewitt charger. *J. Nanoparticle Res.*, *3*: 39–50.
7. Biskos, G.; Reavell, K.; Collings, N. (2005) Unipolar diffusion charging of aerosol particles in the transition regime. *J. Electrostatics*, *36*: 247–265.
8. Laschober, C.; Kaufman, S.L.; Reischl, G.; Allmaier, G.; Szymanski, W.W. (2006) Comparison between an unipolar corona charger and a polonium-based bipolar neutralizer for the analysis of nanosized particles and biopolymers. *J. Nanosci. Nanotechnol.*, *6*: 1474–1481.
9. Alonso, M.; Martin, M.I.; Alguacil, F.J. (2006) The measurement of charging efficiencies and losses of nanoparticles in a corona charger. *J. Electrostatics*, *64*: 203–214.
10. Cheng, S.H.; Ranade, M.B.; Gentry, J.W. (1997) Experimental design of high volume electrostatic charger. *Aerosol Sci. Technol.*, *26*: 433–446.
11. Fuchs, N.A. (1963) On the stationary charge distribution on aerosol particles in a bipolar ionic atmosphere. *Geofis. Pura Appl.*, *56*: 185–193.
12. Asbach, C. (2004) Development and evaluation of a highly efficient gas particle partitioner with minimal effect on the gas composition. Ph. D. thesis, University Duisburg-Essen.

13. Hinds, W.C. (1998) Aerosol Technology, 2nd Ed.; Wiley-Interscience: New York, USA.
14. Tsai, C.J.; Lin, J.S.; Deshpande, C.G.; Liu, L.C. (2006) Electrostatic charge measurement and charge neutralization of fine aerosol particles during generation process. *Part. Part. Sys. Charact.*, *22*: 293–298.
15. Forsyth, B.; Liu, B.Y.H.; Romay, F.J. (1998) Particle charge distribution measurement for commonly generated laboratory aerosols. *Aerosol Sci. Technol.*, *28*: 489–501.
16. Marquard, M.; Meyer, J.; Kasper, G. (2006) Characterization of unipolar electrical aerosol chargers-Part I A review of charger performance criteria. *J. Aerosol Sci.*, *37*: 1052–1068.
17. Alguacil, F.J.; Alonso, M. (2006) Multiple charging of ultrafine particles in a corona charger. *J. Aerosol Sci.*, *37*: 875–884.